

# Geodesic congruences in warped spacetimes

Suman Ghosh <sup>1\*</sup>, Anirvan Dasgupta <sup>2,3 †</sup> and Sayan Kar<sup>1,3 ‡</sup>

<sup>1</sup>*Department of Physics and Meteorology,*

*Indian Institute of Technology,*

*Kharagpur 721 302, India*

<sup>2</sup>*Department of Mechanical Engineering,*

*Indian Institute of Technology,*

*Kharagpur 721 302, India*

<sup>3</sup>*Centre for Theoretical Studies,*

*Indian Institute of Technology,*

*Kharagpur 721 302, India*

---

\* E-mail:suman@cts.iitkgp.ernet.in

† E-mail:anir@cts.iitkgp.ernet.in

‡ E-mail:sayan@cts.iitkgp.ernet.in

## Abstract

In this article, we explore the kinematics of timelike geodesic congruences in warped five dimensional bulk spacetimes, with and without thick or thin branes. We begin our investigations with the simplest case, namely geodesic flows in the Randall–Sundrum AdS (Anti de Sitter) geometry without and with branes. Analytical expressions for the expansion scalar are obtained and the effect of including one or more thin branes (i.e. a background which is a slice of AdS spacetime) on its evolution, is pointed out. Subsequently, we move on to studying such congruences in more general warped bulk geometries with a cosmological thick brane and a time-dependent extra dimensional scale. Using the analytical expressions for the velocity field components, we interpret the expansion, shear and rotation (ESR) along the flows, as functions of the extra dimensional coordinate. The evolution of a cross-sectional area orthogonal to the congruence, as seen from a local observer’s point of view, is also shown graphically. Finally, the Raychaudhuri and geodesic equations in the backgrounds with a thick brane are solved numerically in order to figure out the role of initial conditions (prescribed on the ESR) and spacetime curvature on the evolution of the ESR. Apart from other aspects seen, we specially note the effect of increasing the initial rotation on the delay in appearance of a congruence singularity. This feature is also illustrated through the evolution of a cross sectional area. Our results characterise specific features of timelike geodesic flows which can arise due to warping, the presence/absence of a brane, a cosmological line element and/or a time-dependent extra dimensional scale.

Keywords: Geodesic congruence, Raychaudhuri equation, extra dimension, braneworld.

PACS numbers: 04.50.+h, 12.10.-g

## I. INTRODUCTION

Almost a century ago, in their pioneering research [1], Kaluza and Klein (KK) proposed unification of four dimensional gravity and electromagnetism in a five dimensional gravity framework. This proposal raised a fair amount of curiosity, interest and research activity among theoretical physicists, on the physics of extra dimensions. The idea of extra spatial dimensions appeared in a new incarnation with the advent of Superstring theories [2, 3]. The theoretical existence of branes in String theory eventually motivated the hypothesis that we may be living on an embedded, timelike submanifold (the brane) of a higher dimensional ( $D > 4$ ) Lorentzian spacetime (warped or unwarped), as assumed in the so-called Arkani-Hamed–Dvali–Dimopoulos (ADD) [4, 5] and Randall–Sundrum (RS) [6] braneworld models.

The seminal work of Randall and Sundrum (RS) [6, 7] on warped braneworlds, published a decade ago, refers to the idea of the scale of the extra dimension being spacetime dependent, while addressing the issue of stability, in a two-brane scenario. In a single brane scenario or from a purely higher dimensional bulk perspective, the space-time dependence of the metric function(s) associated with the extra dimensional coordinate(s) basically imply that the scale of the extra dimension depends on the on-brane or four dimensional spacetime coordinates. To visualise this, it is easiest to go back to the early KK universe models with different scale factors associated with the evolution of each set of non-compact/compact dimensions (usual or extra). The difference between today’s warped braneworlds and the KK idea, is the warped geometry and also the non-compact extra dimension(s). Except for a brief discussion on RS type models, we shall, in this article, mostly work with the single brane scenario and a five dimensional bulk.

In earlier papers [8, 9], geodesics in warped spacetimes have been investigated in detail. However, such a study of geodesics alone cannot tell us about the overall local behavior of a family of test particles, as observed in the neighbourhood of a freely falling observer. This motivates us to study the evolution of geodesic congruences. Since the appearance of *Raychaudhuri equations*, in 1955 [10], relativists have discussed and analysed its implications in various contexts. In its original incarnation, the Raychaudhuri equations provided the basis for the description and analysis of spacetime singularities in gravitation and cosmology [11]. For example, the equation for the expansion and the resulting theorem on geodesic focusing, is a crucial ingredient in the proofs of Penrose–Hawking singularity theorems [12,

13].

The kinematics of geodesic congruences is characterised by three kinematical quantities: isotropic expansion, shear and rotation (henceforth referred as ESR) [14–19], which evolve along the flow according to the Raychaudhuri equations. Though mostly quoted and used in the context of gravity, these equations by virtue of their geometric nature, have a much wider scope in studying geodesic as well as non-geodesic flows in nature, which may possibly arise in diverse contexts (see [19] for some open issues). Two of the authors here have recently used these equations to investigate the kinematics of geodesic flows in stringy black hole spacetimes [20] and flows on flat and curved deformable media (including elastic and viscoelastic media) in detail [21, 22].

In this article, we attempt to understand the kinematics of geodesic flows in five dimensional warped bulk spacetimes with and without branes. We begin with a study of the kinematics of geodesic congruences in the simplest bulk—the Randall–Sundrum AdS (Anti de Sitter) spacetime with and without branes. Thereafter, we move on to investigations on geodesic flows in warped bulk spacetimes with a cosmological thick brane and a time–dependent extra dimensional scale. We first obtain the ESR using the geodesic velocity field expressions. The evolution of a cross-sectional area orthogonal to the flow, as seen from a local observer’s frame is also presented. Subsequently, we obtain  $u^A$  as well as the ESR, numerically, by imposing initial conditions on them, and evolving the full system of equations (geodesic and Raychaudhuri) along the flow. This approach (primarily numerical) enables us to obtain the tangent vector field as well as the ESR simultaneously and highlights the role of the initial conditions on all variables. In order to facilitate visualisation, we show the evolution of a cross-sectional area here, as well. Our main motivation behind the work reported here, is to find how the evolution of the ESR are affected by the presence of various metric functions that characterise and distinguish different five dimensional bulk spacetimes with and without thin and thick branes.

Let us assume a bulk line element of the form,

$$ds^2 = e^{2f(\sigma)} [-dt^2 + a^2(t) d\mathbf{X}^2] + b^2(t) d\sigma^2, \quad (1.1)$$

where  $d\mathbf{X}^2 = dx^2 + dy^2 + dz^2$ . Here, the function  $b(t)$  represents the scale of the extra dimension while the  $a(t)$  and  $e^{2f(\sigma)}$  are the usual cosmological scale and warp factors, respectively. We intend to delineate how the features of ESR change when we vary the nature

of each of the three functions  $a(t)$ ,  $b(t)$  and  $f(\sigma)$ . The geodesic equations cannot be solved analytically (modulo a few simplistic cases) in a spacetime as complicated as represented by (1.1). However, first integrals can be found and the ESR may be obtained analytically. For the numerical analysis of the system of differential equations, as detailed in the previous paragraph, we have used standard numerical codes.

Our article is organised as follows. In Section II, we recall the background spacetime geometries, discuss our choices for the various metric functions and review the geodesic equations and first integrals, following our earlier work [8]. In Section III, we first state the definitions of the ESR and write down the evolution (Raychaudhuri) equations for geodesic flows in such a background metric. Further, in Section III-A, we discuss geodesic flows in the Randall Sundrum AdS spacetime with and without branes. Section III-B contains the ESR as found from the definitions, using the velocity field. Here we also discuss the evolution of the cross-sectional area orthogonal to the flow. The numerical analysis of the Raychaudhuri and geodesic equations as an initial value problem is presented in Section III-C. Finally, in Section IV, we summarise our results and conclude with a few remarks.

## II. THE BULK SPACETIMES AND GEODESICS

### A. The bulk spacetimes

The bulk spacetimes we choose to work with are the same as those used in [8]. The line element is given by equation (1.1) rewritten below using the conformal time ( $\eta$ ),

$$ds^2 = e^{2f(\sigma)} a^2(\eta) [-d\eta^2 + d\mathbf{X}^2] + b^2(\eta) d\sigma^2. \quad (2.1)$$

For the purpose of the analysis carried out in the subsequent sections of this article, we must choose the functional forms of the warp factor as well as the cosmological and extra dimensional scale factors. The warp factors  $e^{2f}$  are chosen as,

$$f(\sigma) = \begin{cases} -\ln(\cosh k\sigma) & \rightarrow \text{a decaying warp factor,} \\ \ln(\cosh k\sigma) & \rightarrow \text{a growing warp factor.} \end{cases} \quad (2.2)$$

The above choices are based on the well-known thick brane models [23–25] where the brane is a scalar field domain wall (soliton) in the bulk. The warp factor is therefore a smooth function of the extra dimension. This is different from the RS case where we have  $f(\sigma) =$

$-k|\sigma|$  – a function with a derivative discontinuity, which generates thin branes in the bulk, realised via delta functions in the energy–momentum tensor. We mostly prefer to work with thick branes in order to avoid the discontinuities and delta functions which appear in the connection and curvature, for thin branes. However, as we will see later, in some special cases (e.g. Einstein spaces) one can indeed solve the Raychaudhuri equations consistently, with zero rotation and shear, in the presence of thin branes.

As for the scale factors  $a(\eta)$  and  $b(\eta)$ , we choose them to represent different kinds of time evolution. Our choices are given below, in terms of the cosmological time  $t$ ,

$$\{a(t), b(t)\} = (i) \{a_0 t^{\nu_1}, b_0 + b_1 t^{-\nu_2}\}, \quad \text{and} \quad (ii) \{a'_0 e^{H(t-t_0)}, b'_0 + b'_1 e^{-\beta H(t-t_0)}\}. \quad (2.3)$$

In the above,  $\nu_1$  spans over an open interval  $(0, 1)$ . Thus, in (i)  $a(t)$  represents an expanding but decelerating on–brane line element (which is radiative for  $\nu_1 = \frac{1}{2}$ ), while in (ii) we assume  $H$  to be positive, thereby representing an accelerating de–Sitter on–brane line element.  $b_0, b_1, \nu_2, b'_0, b'_1$  and  $\beta$  are positive so that we have a decaying extra dimension which stabilizes to a finite value as  $t \rightarrow \infty$ . The metric functions mentioned above may be obtained as solutions of the five dimensional Einstein equations with the corresponding Einstein tensors providing matter energy-momentum profiles. As shown in [26], for similar metric functions, the matter stress-energy can satisfy the Weak Energy Condition. It may be noted that these models are assumed to represent the evolution of the universe beginning at a finite time  $t = t_0 (\neq 0)$  when both the scales of visible and extra dimension were same.

Using conformal time, the scale factors in set (i) and set (ii) can be re-expressed as [8]

$$a(\eta) = \frac{t_0}{1 - \nu_1} \eta^{\frac{\nu_1}{1 - \nu_1}}, \quad b(\eta) = t_0 \left( \frac{\nu_1}{1 - \nu_1} + \eta^{\frac{-\nu_2}{1 - \nu_1}} \right), \quad 1 \leq \eta \leq \infty \quad (2.4)$$

and

$$a(\eta) = \frac{1}{H} \frac{1}{(1 - \eta)} \quad b(\eta) = \frac{1}{H} \left[ 1 - b'_1 H \{1 - (1 - \eta)^\beta\} \right], \quad 0 \leq \eta \leq 1 \quad (2.5)$$

respectively. As a specific case, let us consider,  $\nu_1 = \nu_2 = \frac{1}{2}$ ,  $t_0 = 1$ ,  $H = 1$ ,  $b'_1 = \frac{1}{2}$  and  $\beta = 1$  which leads to the following two different combinations of the scale factors,

$$\begin{aligned} \text{(A)} \quad & a(\eta) = 2\eta, \quad b(\eta) = 1 + \frac{1}{\eta}, \\ \text{(B)} \quad & a(\eta) = \frac{1}{1 - \eta}, \quad b(\eta) = 1 - \frac{\eta}{2}. \end{aligned}$$

The above combinations of scale factors are referred to as Set(A) and Set(B) in the later sections.

## B. Geodesic equations and first integrals

In this brief subsection, we quickly review the geodesics following [8], with the aim of writing down the first integrals of geodesic motion, which will be used in later sections. The constraint  $g_{AB}u^A u^B = -\epsilon$ , for null and timelike geodesics in the line element (2.1) is given as

$$e^{2f(\sigma)}a^2(\eta) [-\dot{\eta}^2 + \dot{\mathbf{X}}^2] + b(\eta)^2 \dot{\sigma}^2 + \epsilon = 0, \quad (2.6)$$

where  $\epsilon = 1$  and  $0$  correspond to timelike and null geodesics, respectively. A dot here represents differentiation with respect to the affine parameter  $\lambda$ . Since  $x_i$  is cyclic for geodesics in 2.1, we have

$$\dot{x}_i = \frac{C_i e^{-2f}}{a^2}, \quad (2.7)$$

where  $C_i$ 's are integration constants. The full geodesic equations

$$\frac{d^2 x^A}{d\lambda^2} + \Gamma_{CD}^A \frac{dx^C}{d\lambda} \frac{dx^D}{d\lambda} = 0 \quad (2.8)$$

in a spacetime corresponding to the metric (2.1) are almost impossible to solve analytically. However, the set of equations in Eq.2.8 may be recast as the following first order dynamical system of coupled, ordinary, first order differential equations [8],

$$\dot{\eta} = \frac{e^{-f(\sigma)}}{a(\eta)} \sqrt{\epsilon + \frac{\sum_{i=1}^3 C_i^2}{e^{2f(\sigma)} a^2(\eta)} + \frac{\chi^2}{b^2(\eta)}}, \quad (2.9)$$

$$\dot{x}_i = \frac{C_i e^{-2f(\sigma)}}{a^2(\eta)}, \quad (2.10)$$

$$\dot{\sigma} = \frac{\chi}{b^2(\eta)}, \quad (2.11)$$

$$\text{and } \dot{\chi} = -f'(\sigma) \left( \epsilon + \frac{\chi^2}{b^2(\eta)} \right). \quad (2.12)$$

by defining a new quantity  $\chi(\lambda)$  given by Eq.2.11. Here the dots represent differentiation with respect to the affine parameter  $\lambda$ , while primes denote differentiation of the respective functions, with respect to their corresponding independent variables,  $\eta$  or  $\sigma$ . Thus, for simple cases, one can find the first integrals of the geodesic equations directly from the above relations and these can then be used to determine the ESR.

### III. RAYCHAUDHURI EQUATION AND ESR VARIABLES

To quantify the different kinematical quantities that characterize the flow of a geodesic congruence (family of non-intersecting integral curves generated by a given geodesic vector field) in a given background spacetime, the gradient of the velocity field is split into following three parts,

$$\nabla_B u_A = \Sigma_{AB} + \Omega_{AB} + \frac{1}{n-1} h_{AB} \Theta, \quad (3.1)$$

where,  $n$  is the dimension of spacetime and  $h_{AB} = g_{AB} \pm u_A u_B$  is the projection tensor (the plus sign is for timelike curves whereas the minus one is for spacelike ones) and  $u_A u^A = \mp 1$ .  $\Theta$ , the trace of  $\nabla_B u_A$ , represents the isotropic expansion,  $\Sigma_{AB}$  is the symmetric, traceless part representing the shear and  $\Omega_{AB}$  are the components of the antisymmetric rotation tensor. Therefore, by definition

$$\Theta = \nabla_A u^A, \quad (3.2)$$

$$\Sigma_{AB} = \frac{1}{2} (\nabla_B u_A + \nabla_A u_B) - \frac{1}{n-1} h_{AB} \Theta, \quad (3.3)$$

$$\Omega_{AB} = \frac{1}{2} (\nabla_B u_A - \nabla_A u_B). \quad (3.4)$$

It is interesting to note that for geodesic congruences with zero rotation, one can always write  $u_A = \partial_A \Phi$ , where  $\Phi(x^A)$  is a scalar function. Thus, the expansion scalar can be redefined as  $\Theta = \square \Phi$ . One can find this scalar function by integrating the velocity vector field. One such example is shown later.

We now turn towards writing down the evolution equations for the expansion, shear and rotation along the flow, representing a timelike geodesic congruence. A fact worth mentioning here is that, these evolution equations (and their generalisations) are essentially *geometric statements* and are independent of any reference to the Einstein field equations.

The modern (textbook) way to derive these equations (see [15]) is as follows. Consider the quantity  $u^C \nabla_C B_{AB}$  (where  $B_{AB} = \nabla_B u_A$ ). Evaluating this as an identity we get

$$u^C \nabla_C B_{AB} = -B_{AC} B_B^C - R_{ACBD} u^C u^D. \quad (3.5)$$

Then splitting the above equation into its trace, symmetric traceless and anti-symmetric parts, we have

$$\frac{d\Theta}{d\lambda} + \frac{1}{n-1} \Theta^2 + \Sigma^2 - \Omega^2 = -R_{AB} u^A u^B \quad (3.6)$$



$$u^C \nabla_C \Sigma_{AB} = -\frac{2}{n-1} \Theta \Sigma_{AB} - \Sigma_{AC} \Sigma_B^C - \Omega_{AC} \Omega_B^C + \frac{1}{n-1} h_{AB} (\Sigma^2 - \Omega^2) \\ + W_{CBAD} u^C u^D + \frac{1}{n-2} \tilde{R}_{AB} \quad (3.7)$$

$$u^C \nabla_C \Omega_{AB} = -\frac{2}{n-1} \Theta \Omega_{AB} - 2 \Sigma_{[B}^C \Omega_{A]C} \quad (3.8)$$

where  $\Sigma^2 = \Sigma_{AB} \Sigma^{AB}$ ,  $\Omega^2 = \Omega_{AB} \Omega^{AB}$ ,  $W_{CBAD}$  is the Weyl tensor and the quantity  $\tilde{R}_{AB} = h_{AC} h_{BD} R^{CD} - \frac{1}{n-1} h_{AB} h_{CD} R^{CD}$ . One can analyse the above equations for special cases, as we shall see below.

### A. Randall–Sundrum warp factor with and without branes

It is known that in Einstein spaces, we have  $R_{AB} \sim g_{AB}$  and all the components of the Weyl tensor as well as  $\tilde{R}_{AB}$  vanish. Therefore the equation for the expansion simplifies considerably if we set  $\Sigma_{AB} = \Omega_{AB} = 0 \forall A, B$ . Following this prescription for the RS scenario [6, 7] in the absence of any brane, Eq. 3.6 gives us

$$\frac{d\Theta}{d\lambda} + \frac{\Theta^2}{4} = \frac{\Lambda}{6M^3} \quad (3.9)$$

where,  $\Lambda$  is the bulk cosmological constant and  $M$  is the five dimensional Planck mass. Let us further assume  $\Theta = 4 \frac{\dot{F}}{F}$  (notion of focusing is related to  $F = 0$ ,  $\dot{F} < 0$  at finite  $\lambda$ ), which leads to

$$\ddot{F} + k^2 F = 0, \quad \text{with} \quad k = \sqrt{\frac{-\Lambda}{24M^3}}, \quad (3.10)$$

As discussed in [7],  $\Lambda$  has to be negative. Eq.3.10 has simple oscillatory solutions such as  $c_1 \sin(k\lambda + c_2)$ , which imply  $\Theta = 4k \cot(k\lambda + c_2)$ . Therefore, the nature of focusing or defocusing of geodesics in the bulk depends on the initial condition or the value of  $c_2$ . However, this is the behavior of geodesic congruences in the bulk with no branes. If we introduce two 3-branes, the hidden brane (with positive tension  $24M^3 k$ ) at  $\sigma = 0$  and the visible brane (with equal negative tension) at  $\sigma = \pi$ , Eq.3.10 becomes

$$\ddot{F} + [k^2 + 2k\{\delta(\sigma) - \delta(\sigma - \pi)\}] F = 0. \quad (3.11)$$

Using the following property of Dirac delta function

$$\delta(\sigma(\lambda)) = \sum_i \frac{\delta(\lambda - \lambda_i)}{|\dot{\sigma}(\lambda_i)|}, \quad (3.12)$$

and the first integral of the  $\sigma$  geodesic equation

$$\dot{\sigma} = \sqrt{C^2 e^{-2f} - 1} \quad \text{with} \quad f(\sigma) = -k|\sigma|, \quad (3.13)$$

we arrive at

$$\ddot{F} + [k^2 + k_1\delta(\lambda - \lambda_0) - k_2\delta(\lambda - \lambda_\pi)] F = 0, \quad (3.14)$$

where,  $k_1 = \frac{2k}{\sqrt{C^2-1}}$ ,  $k_2 = \frac{2k}{\sqrt{C^2 e^{2k\pi}-1}}$ ,  $\lambda_0 = \frac{\sec^{-1} C}{k}$  and  $\lambda_\pi = \frac{\tan^{-1} \sqrt{C^2 e^{2k\pi}-1}}{k}$ . The solution of the above equation is given by [27]

$$F(\lambda) = c_1 \sin(k\lambda + c_2) + c_3 e^{-\alpha|\lambda-\lambda_0|} + c_4 e^{-\alpha|\lambda-\lambda_\pi|} \quad (3.15)$$

where  $c_1, c_2, c_3, c_4$  are arbitrary constants. We then integrate the second order equation for  $F$ , around the neighborhood of  $\lambda_0$  and  $\lambda_\pi$  to obtain two algebraic equations for  $c_1$  and  $c_2$ . The determinant condition for nontrivial solutions of  $c_1, c_2$  yields the following transcendental equation,

$$(2\alpha - k_1)(2\alpha + k_2) + k_1 k_2 e^{-2\alpha(\lambda_\pi - \lambda_0)} = 0. \quad (3.16)$$

from which  $\alpha$  can be obtained numerically. In our case,  $\alpha \sim k_1/2$  is a good approximation (we have checked this with numerical solutions as well). Fig.1 shows (shaded regions) the domain of the parameters  $c_3/c_1$  and  $c_4/c_1$  ( $c_2$  is taken to be zero), in cases where  $F = 0$  at some finite value of  $\lambda$  between the two branes. Points on the boundaries of the shaded regions correspond to the occurrence of  $F = 0$  at the location of the branes (i.e.  $\lambda = \lambda_0, \lambda = \lambda_\pi$  and the corresponding  $\sigma$  through the function  $\sigma(\lambda)$ ). In the lightly shaded region,  $\dot{F} > 0$ , which implies complete defocusing of geodesics ( $\theta \rightarrow +\infty$ ) at finite  $\lambda$ , whereas in the darker region,  $\dot{F} < 0$ , i.e. geodesic focusing ( $\theta \rightarrow -\infty$ ) is possible. Note that different values for  $c_2$  will result in different parameter space diagrams involving the quantities  $c_3/c_1$  and  $c_4/c_1$ . Eq.3.15 leads to the modified expansion scalar, due to the presence of the branes, as given by

$$\Theta(\lambda) = 4 \frac{c_1 k \cos(k\lambda + c_2) - c_3 \alpha \operatorname{sgn}(\lambda - \lambda_0) e^{-\alpha|\lambda-\lambda_0|} - c_4 \alpha \operatorname{sgn}(\lambda - \lambda_\pi) e^{-\alpha|\lambda-\lambda_\pi|}}{c_1 \sin(k\lambda + c_2) + c_3 e^{-\alpha|\lambda-\lambda_0|} + c_4 e^{-\alpha|\lambda-\lambda_\pi|}}. \quad (3.17)$$

Due to the new integration constants, the behavior of geodesic congruences have become much richer. In Fig.2(a) and Fig.2(b) two such examples are shown using typical values (points represented by the black and white dots in Fig.1) of the parameters and constants. It is clear from these figures, how the existence of branes modifies the expansion profiles.

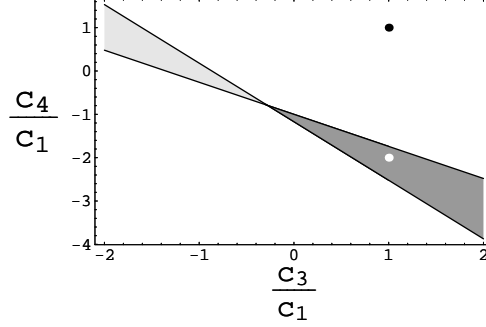
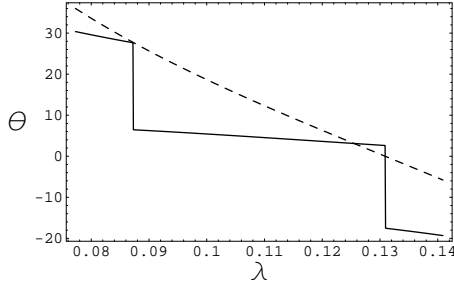
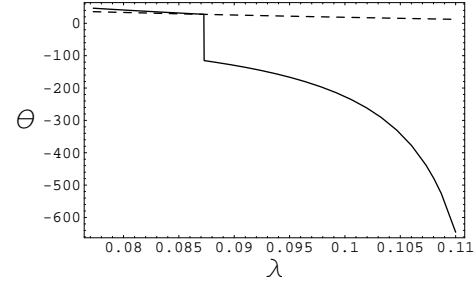


FIG. 1: Values of  $c_3/c_1$  and  $c_4/c_1$  lying in the shaded region corresponds to focusing (deeply shaded region) and defocusing (lightly shaded region) of geodesics in between the branes with  $k = 12$ ,  $C = 2$ ,  $\lambda_0 = 0.087$  (1st brane location),  $\lambda_\pi = 0.131$  (2nd brane location),  $c_2 = 0$  and  $\alpha = 6.9282$  (from Eq.3.16).



(a)  $c_3 = c_4 = 1$  : corresponds to the black dot in Fig.1



(b)  $c_3 = 1$  and  $c_4 = -2$  : corresponds to the white dot in Fig.1

FIG. 2: Evolution of expansion scalar in presence (continuous line) and in absence (dotted line) of two 3-branes with  $k = 12$ ,  $C = 2$ ,  $c_1 = 1$ ,  $c_2 = 0$  and  $\alpha = 6.9282$  while the branes are located at  $\lambda_0 = 0.087$  and  $\lambda_\pi = 0.131$ .

After this brief discussion on geodesic flows in the RSI scenario, we will now address the problem of solving the Raychaudhuri equations in a generalised braneworld scenario, with a thick cosmological brane and a time dependent extra dimension. Our main aim is to point out the specific roles of the different metric functions (which appear in the line element) on the evolution of geodesic congruences.

## B. ESR from definitions

As mentioned before, one can derive analytic expressions for the ESR variables directly from the definitions, Eq.3.2 - Eq.3.4, using the geodesic vector field components obtained in Section II. We now illustrate the nature of the ESR for some specific cases, where we take one or two of the metric functions as constants.

### 1. Case 1

With  $a(\eta) = b(\eta) = \text{constant}$ , the line element is given by

$$ds^2 = e^{2f(\sigma)} [-d\eta^2 + d\mathbf{X}^2] + d\sigma^2, \quad (3.18)$$

and the corresponding velocity vector components for timelike geodesics are given by

$$u^\alpha = C_\alpha e^{-2f} \quad \text{where} \quad \alpha = 0, 1, 2, 3 \quad (3.19)$$

$$u^4 = \sqrt{C^2 e^{-2f} - 1} \quad \text{where} \quad C^2 = C_0^2 - \sum_{i=1}^3 C_i^2, \quad (3.20)$$

where the  $C_\alpha$ 's are integration constants, which are constrained by the fact that  $u^4$  has to be real valued. Fig.3, following [8], shows the nature of timelike geodesics in the presence of growing and decaying warp factors. Clearly, the geodesics are bounded along the  $\sigma$  direction in the case of a growing warp factor and the boundaries are given by  $|\sigma| = \text{sech}^{-1}(1/C)$ . However this is not the situation with a decaying warp factor, though  $\lambda$  itself is bounded. For a detailed study of geodesics in generalised braneworld scenarios, see [8]. The scalar

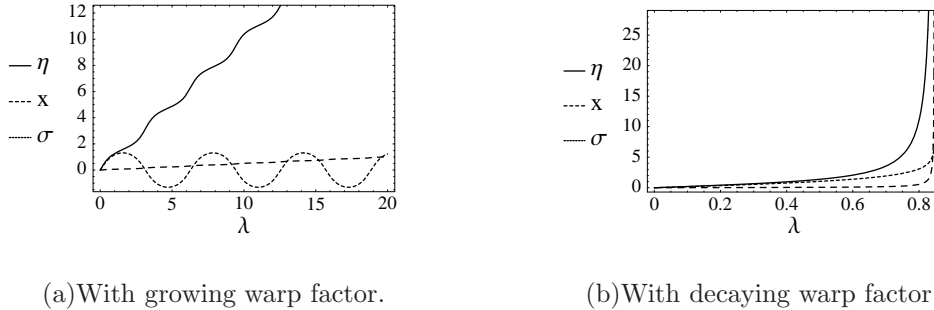


FIG. 3: Evolution of the components of timelike geodesics for growing and decaying warp factors with both  $a(\eta) = b(\eta) = \text{constant}$ .

function,  $\Phi$ , defined in the previous section, for the case with a decaying warp factor is given

by

$$\Phi(x^A) = \sum_{\alpha=0}^3 C_\alpha x^\alpha - i\sqrt{C^2 - 1} \text{EllipticE} \left[ i\sigma, \frac{C^2}{C^2 - 1} \right] + C_4, \quad (3.21)$$

where  $C_4$  is an integration constant. Similarly, one can find this scalar for other cases too, as long as the rotation is zero.

According to the definitions Eq.3.2 - Eq.3.4, the expansion scalar and the other ESR variables for a congruence of timelike geodesics, written as functions of  $\sigma$ , are given as follows,

$$\begin{aligned} \Theta &= \frac{3C^2 e^{-2f} - 4}{\sqrt{C^2 e^{-2f} - 1}} f', \\ \Sigma_{00} &= \frac{C_0^2(4 - 3C^2 e^{-2f}) - C^2}{4\sqrt{C^2 e^{-2f} - 1}} f', \quad \Sigma_{ii} = \frac{C_i^2(4 - 3C^2 e^{-2f}) + C^2}{4\sqrt{C^2 e^{-2f} - 1}} f', \\ \Sigma_{44} &= -\frac{3C^4 f' e^{-4f}}{4\sqrt{C^2 e^{-2f} - 1}}, \quad \Sigma_{\alpha i} = -\frac{C_\alpha C_i(3C^2 e^{-2f} - 4)}{4\sqrt{C^2 e^{-2f} - 1}} f' \text{ for } \alpha \neq i, \\ \Sigma_{\alpha 4} &= -\frac{C_\alpha}{4} 3C^2 f' e^{-2f}, \quad \Sigma^2 = \frac{3C^4 e^{-4f} f'^2}{4(C^2 e^{-2f} - 1)} \quad \text{and} \quad \Omega_{AB} = 0 \forall A, B. \end{aligned} \quad (3.23)$$

It may be mentioned here that above expressions do satisfy Eq.3.6.

For the chosen growing and decaying warp factors respectively, the expansion scalar becomes

$$\Theta_+ = \frac{3C^2 \text{sech}^2 \sigma - 4}{\sqrt{C^2 \text{sech}^2 \sigma - 1}} \tanh \sigma \quad \text{and} \quad \Theta_- = -\frac{3C^2 \cosh^2 \sigma - 4}{\sqrt{C^2 \cosh^2 \sigma - 1}} \tanh \sigma. \quad (3.24)$$

It can be easily seen that, in the region  $\dot{\sigma} > 0$ , irrespective of the value of  $C$ ,  $\Theta_\pm \rightarrow -\infty$  as  $\sigma$  increases. Therefore a geodesic congruence singularity arises in both the cases. With  $\Theta_+$ , if  $C > \sqrt{4/3}$ , initially the expansion remains positive but eventually geodesics meet exactly at the boundary of the accessible domain along the extra dimension because the velocity component along  $\sigma$ ,  $u^4$ , which appears in the denominator in the expression for  $\Theta$ , vanishes at that point (and also changes sign). With  $\Theta_-$ , the geodesic congruence singularity appears as  $\sigma \rightarrow \infty$ . For  $\dot{\sigma} < 0$  an exactly similar behavior is obtained. The following figures (Fig.4 and Fig.5) illustrate the nature of the expansion and shear in the presence of growing and decaying warp factors. From the corresponding geodesics shown in Fig.3 we note that  $\Theta_+$  experiences a finite time singularity (i.e. finite  $\lambda$  as well as finite  $\sigma$ ) but  $\Theta_-$  becomes singular at finite  $\lambda$  but  $\eta, \sigma \rightarrow \infty$ . The continuous and dashed curves in the plots of  $\Theta$  vs.  $\sigma$  stand for geodesics with positive  $u^4$  (moving towards positive  $\sigma$  direction) and negative  $u^4$  (moving towards negative  $\sigma$  direction), respectively. In both cases congruence singularities

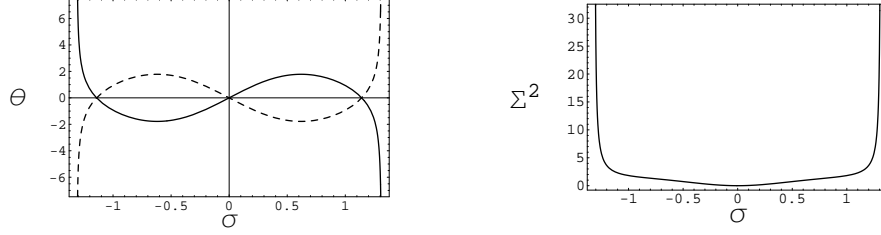


FIG. 4: Nature of expansion ( $\dot{\sigma} > 0$ : continuous,  $\dot{\sigma} < 0$ : dashed) and shear in presence of growing warp factor with  $C = 1.31$ .

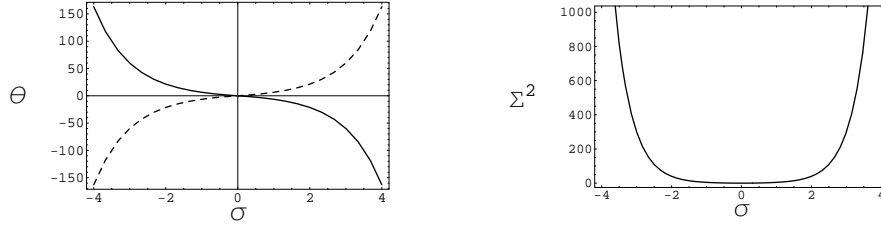


FIG. 5: Nature of expansion ( $\dot{\sigma} > 0$ : continuous,  $\dot{\sigma} < 0$ : dashed) and shear in presence of decaying warp factor with  $C = 1.31$ .

are inevitable. The evolution of  $\Sigma^2$  in these scenarios, plotted in Fig.4 and Fig.5, follow from its expression as given in Eq.3.23.

To understand how geodesic congruences behave in all the abovementioned scenarios, let us consider the evolution of the projections of the cross-sectional area orthogonal to the flow lines, of a congruence of four geodesics, on different two dimensional surfaces. This is done by numerically solving the following equation for the deviation vector along with Eq.3.5 and Eq.2.8,

$$\xi^A_{;B} u^B = B^A_B \xi^B. \quad (3.25)$$

Here,  $\xi^A$  represents the separation between two neighboring geodesics. To see the evolution from a local observer's viewpoint, we have to express the tensorial quantities in the frame basis. The metric tensor in coordinate basis and frame basis are related as

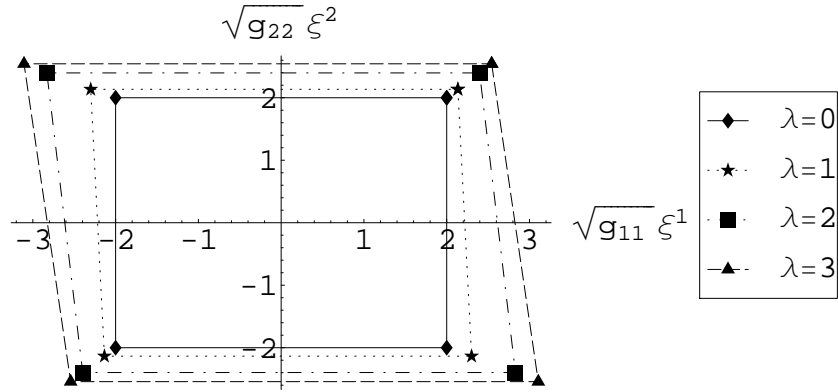
$$g^{AB} = e^A_a e^B_b \eta^{ab}, \quad (3.26)$$

where the vierbein field,  $e^A_a$ , has two indices, “ $A$ ” labels the general spacetime coordinate (w.r.t. the coordinate basis) and “ $a$ ” labels the local Lorentz spacetime or local laboratory coordinates (w.r.t. the frame basis). The tensorial components in these two bases are related

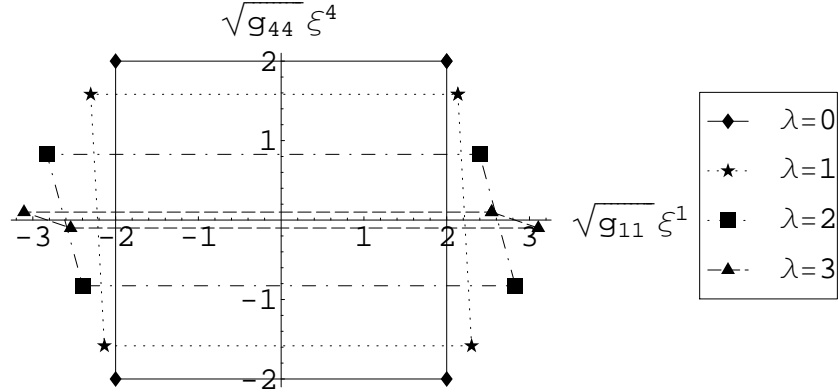
as

$$\xi^A = e^A_a \xi^a. \quad (3.27)$$

In the frame basis, we set the initial conditions such that, at  $\lambda = 0$ , the projected area has the shape of a square in the  $\sqrt{g_{11}}\xi^1$ - $\sqrt{g_{22}}\xi^2$  plane or in the  $\sqrt{g_{11}}\xi^1$ - $\sqrt{g_{44}}\xi^4$  plane where  $\xi$ 's are essentially solutions of Eq.3.25. The following figures (Fig.6) show the evolution of the area elements as  $\lambda$  increases. The origin represents the location of the observer. We have chosen initial conditions such that all components of the rotation vanish.



(a) Evolution of the projected square element on  $\sqrt{g_{11}}\xi^1$ - $\sqrt{g_{22}}\xi^2$  plane

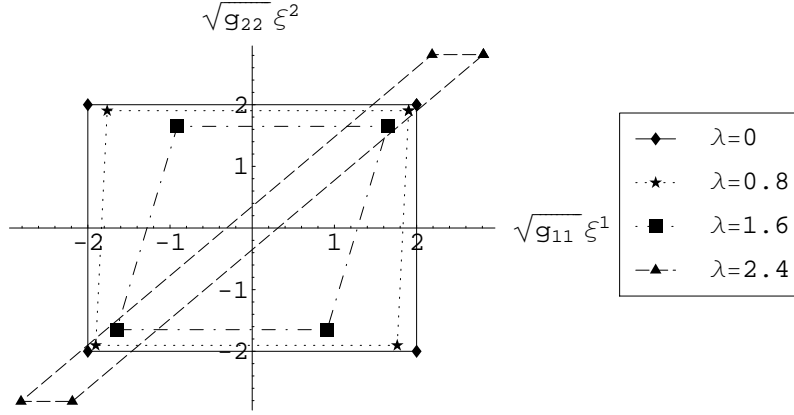


(b) Evolution of the projected square element on  $\sqrt{g_{11}}\xi^1$ - $\sqrt{g_{44}}\xi^4$  plane

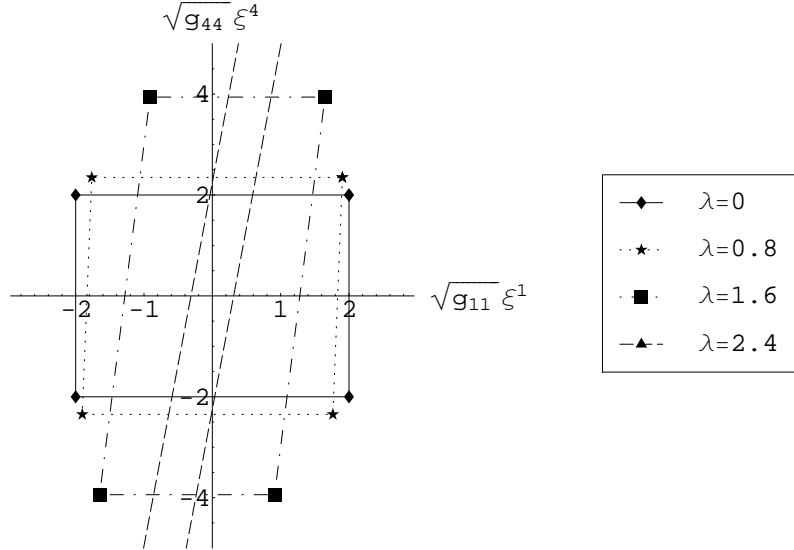
FIG. 6: Evolution of different 2D surface elements in Case 1 in presence of a growing warp factor

Fig.6 shows how a projected 2D square element evolves, in a static bulk, in presence of a growing warp factor i.e. the scenario addressed in Fig.4. In Fig.6(a), the initial square area (at  $\lambda = 0$ ) in the  $\sqrt{g_{11}}\xi^1$ - $\sqrt{g_{22}}\xi^2$  plane expands and distorts slightly and converges

on a parallelogram at  $\lambda \sim 3.14$ . In Fig.6(b), however the area in the  $\sqrt{g_{11}}\xi^1$ - $\sqrt{g_{44}}\xi^4$  plane shrinks, distorts and converges on the  $\sqrt{g_{11}}\xi^1$  axis at  $\lambda \sim 3.14$ , clearly suggesting focusing along the extra dimension. The effect of shear is evident from the evolution of the shape of the area. From Fig.3 we note that the geodesics turn around at the boundary ( $\sigma(\lambda)$ , reach a maximum at  $\lambda \sim 3.14$ ) and oscillate along the extra dimension (duration between  $\lambda = 0$  and  $\lambda = 3.14$  corresponds to one-fourth of a period of oscillation of  $\sigma(\lambda)$ ).



(a) Evolution of the projected square element on  $\sqrt{g_{11}}\xi^1$ - $\sqrt{g_{22}}\xi^2$  plane



(b) Evolution of the projected square element on  $\sqrt{g_{11}}\xi^1$ - $\sqrt{g_{44}}\xi^4$  plane

FIG. 7: Evolution of different 2D surface elements in Case 1 in presence of a decaying warp factor.



On the other hand, Fig.7 corresponds to the scenario shown in Fig.5, where the warp factor is of decaying type. In Fig.7(a), shrinking of the area element is quite prominent whereas in Fig.7(b) it is not so. However, in both the figures, the square area becomes more and more parallelogram shaped and eventually converge on a line  $\sqrt{g_{11}}\xi^1 \propto \sqrt{g_{22}}\xi^2$  or  $\sqrt{g_{11}}\xi^1 \propto \sqrt{g_{44}}\xi^4$  as  $\lambda \rightarrow \infty$ .

The nature of evolution of the square elements is therefore a distinguishing feature between bulk universes with growing and decaying warp factors. It is worth mentioning here that, to a brane based observer, only the evolution depicted in Fig.6(a) or Fig.7(a) will be visible whereas congruence singularities realised in Fig.6(b) or Fig.7(b) will remain unnoticed. In a way, therefore, one can find the nature of warping as well as the existence of extra dimensions from the evolution pattern of cross-sectional area elements.

## 2. Case 2

Next, we consider the case where  $f(\sigma) = \text{constant}$ . The line element now looks like

$$ds^2 = a^2(\eta) [-d\eta^2 + d\mathbf{X}^2] + b^2(\eta) d\sigma^2. \quad (3.28)$$

Integral curves are given by the following velocity vector field

$$\begin{aligned} u^i &= \frac{C_i}{a^2}, & u^4 &= \frac{C_4}{b^2}, \\ u^0 &= \sqrt{\frac{1}{a^2} + \sum_{i=1}^3 \frac{C_i^2}{a^4} + \frac{C_4^2}{a^2 b^2}} \end{aligned} \quad (3.29)$$

We can calculate the expansion scalar which turns out to be,

$$\Theta = -\frac{1}{u_0} \left[ 3\frac{\dot{a}}{a} + 2\sum_i \frac{C_i^2 \dot{a}}{a^3} + \frac{3C_4^2 \dot{a}}{ab^2} + \frac{\dot{b}}{b} + \sum_i \frac{C_i^2 \dot{b}}{a^2 b} \right]. \quad (3.30)$$

As done before one can also find the components of the shear tensor (not shown here). The rotation tensor components are zero, as is evident from the velocity field. Fig.8 and Fig.9 show the evolution of expansion scalar and  $\Sigma^2$  as functions of  $\eta$  for two different  $a(\eta), b(\eta)$  combinations i.e. Set(A) and Set(B), respectively. In Fig.8 (Set(A)), geodesics become parallel as  $\eta \rightarrow \infty$ . This is because with Set(A), expansion of the universe itself slows down with increasing  $\eta$  (it is worth mentioning here that as the cosmological evolution is assumed to begin at a finite  $\eta$ , the past singularity will not appear here since it corresponds

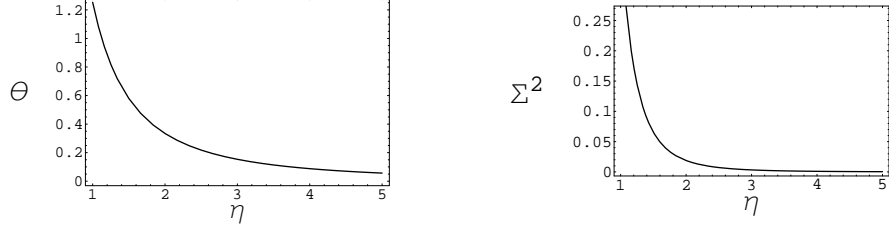


FIG. 8: Nature of expansion and shear in Case 2 for Set(A), with  $C_i = C_4 = 0.1$

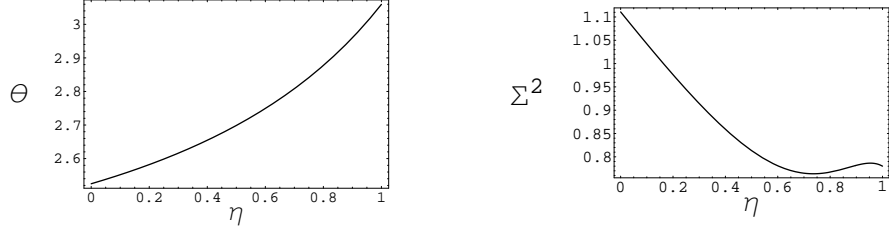


FIG. 9: Nature of expansion and shear in Case 2 for Set(B), with  $C_i = C_4 = 0.1$

to  $\eta = 0$  and falls outside the domain of  $\eta$  for the models considered in this article). For Set(B), Fig.9 demonstrates that the geodesics spread apart at an ever increasing rate with increasing  $\eta$  – this is due to very rapid (exponential in real time) expansion of the universe. In both these cases geodesic focusing is not achieved. On the other hand, as noted in the previous subsection, geodesic singularities are unavoidable when a non-constant warp factor is assumed. Therefore, it should be interesting to see how these two apparently opposite features compete with each other when we consider the full braneworld geometry with all three non-constant metric functions present.

We end this subsection by trying to figure out the individual effect of the dynamic nature of  $b(\eta)$ . Assuming  $a(\eta)$  as constant in Eq.3.30 we get,

$$\Theta = \frac{(1 + \sum_i C_i^2) \dot{b}}{\sqrt{(1 + \sum_i C_i^2) b^2 + C_4^2}}. \quad (3.31)$$

In our models  $\dot{b}$  is negative and as  $\eta$  increases it tends to zero. For the  $b(\eta)$  of Set(A),  $\Theta$  tends to zero i.e. geodesics become parallel while for Set(B) it converges to a finite value which implies that the geodesics keep moving away from each other at an approximately steady rate. So, with only a  $b(\eta)$ , in both the above Sets (A) and (B), geodesic focusing never happens. It is interesting to note that even if  $b(\eta) \rightarrow 0$  i.e. size of the extra dimension becomes singular the expansion scalar remains finite as long as  $\dot{b}$  is finite. Therefore we

expect  $b(\eta)$  to play a role only in introducing a scaling effect. This will become clearer in the next section, when we consider the general scenario where all the three non-constant metric functions are considered.

One may ask—what about analytic expressions for the kinematic variables in the general case? Analytic expressions for the first integrals of the geodesic equations for the case with both  $f(\sigma)$  and  $a(\eta)$  present can also be found easily. However, in this case, the ESR variables as obtained from the definitions given in Eq.3.2-3.4 are functions of both  $\sigma$  and  $\eta$ . Further they cannot be reduced to explicit functions of  $\lambda$  (or  $\sigma$ ,  $\eta$ ) alone. This happens because we do not know how  $\sigma(\lambda)$  and  $\eta(\lambda)$  are related to each other (analytically). Thus, the above two subcases (of a generalised braneworld geometry) are the only ones where one can find useful, closed-form analytic expressions for the ESR variables, directly from the geodesic velocity vector field.

### C. Numerical solutions

Let us briefly state the methodology behind our numerical work. We shall numerically solve Eq.3.5 simultaneously with Eq.2.8 for different combinations of the metric functions, in order to understand the interplay amongst all the terms appearing in the Raychaudhuri equations. Looking at Eq.3.6, one sees that, the “ $\Omega^2$ ” term has an opposite effect as compared to the shear term. Thus, it may play a role in avoiding/delaying congruence singularities found in the earlier section. On the other hand, as we shall see, the curvature term “ $R_{AB}u^A u^B$ ”, in Eq.3.6, also has a significant effect on ESR profiles through its large positive or negative value at a given spacetime point.

We have analysed each case for two types of initial conditions – one with zero rotation and one with very high initial rotation, keeping initial  $\Theta$  and  $\Sigma_{AB}$  as zero. Non-zero initial values for  $\Omega_{AB}$  are chosen such that  $\Omega_{AB}u^B = 0 = u^A\Omega_{AB}$  at  $\lambda = 0$ . Initial velocities for cases involving Set(A) scale factors are taken as  $\{0.728, 0.1, 0.1, 0.1, 0.5\}$ , whereas for Set(B), it is assumed as  $\{1.1314, 0.1, 0.1, 0.1, 0.5\}$  so that the timelike constraint is satisfied. Let us now understand the results through the various plots. In the following figures (Fig.10-Fig.13), the subfigures (a) and (b) contain *dual-axis* plots where the continuous curves (axes) represent evolution with zero initial rotation and the dashed curves (axes) represent evolution with high initial rotation.

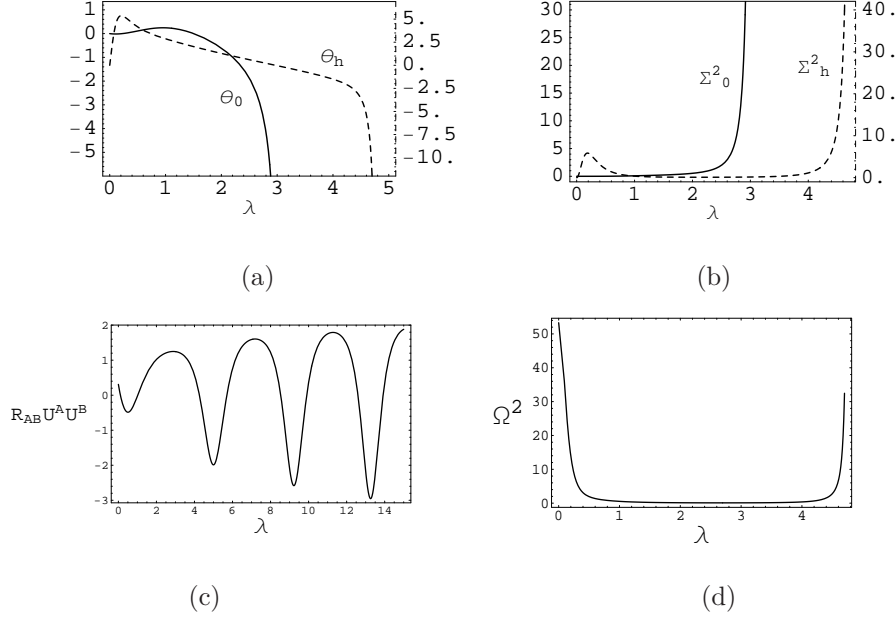


FIG. 10: Nature of expansion, shear and rotation for  $f(\sigma) = \log(\cosh \sigma)$ ,  $a(\eta) = 2\eta$  and  $b(\eta) = 1 + 1/\eta$  with two different set of initial conditions. In (a) and (b), subscripts 0 ( $h$ ) correspond to zero (high) initial rotation.

We now describe each figure and mention the salient features observed in them.

Fig.10: In the presence of a growing warp factor, a radiative brane and an asymptotically static extra dimension, geodesic congruences without any initial rotation, expand slowly at first but later become focused at a finite  $\lambda$ . The shear ( $\Sigma^2$ ) grows indefinitely. When high initial rotation is introduced, expansion inflates for a very short while but eventually the geodesics gets focused again at another finite but larger value of  $\lambda$ . Though rotation increases at late times, it is always dominated by shear, which grows even faster. Initial rotation only succeeds in delaying the focusing. The curvature term, as we note, is not an important factor here.

Fig.11: In the presence of a decaying warp factor, a radiative brane and an asymptotically static extra dimension the geodesics, without any initial rotation, do come closer to each other monotonically, but focus only at  $\sigma \rightarrow \infty$ . The shear grows indefinitely. When high initial rotation is introduced, the congruence expands initially but eventually geodesics tend to focus again asymptotically. The curvature term becomes large positive valued and thus always seems to help in the occurrence of congruence singularity.

Fig.12 represents almost the same behavior as seen in Fig.10. But here the large initial

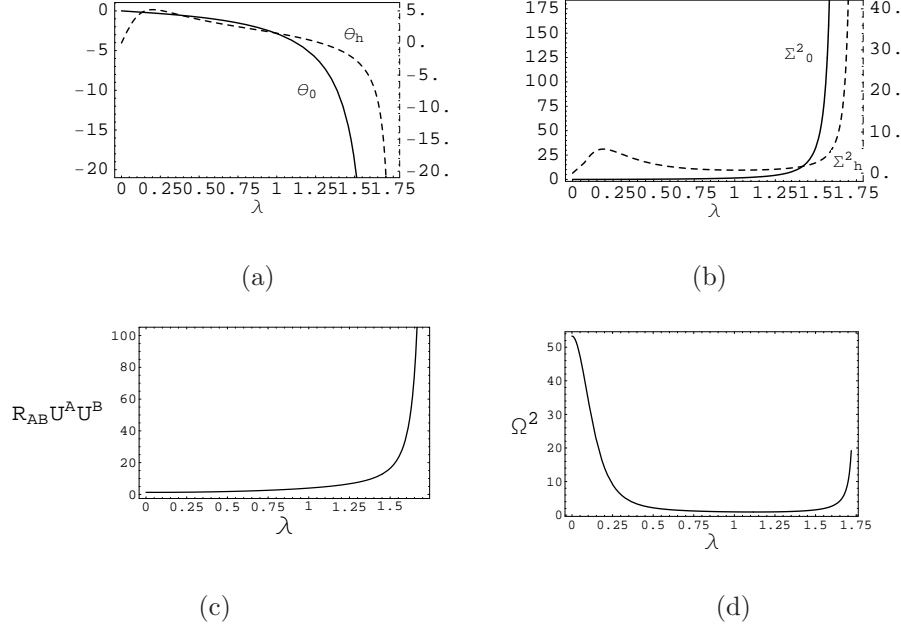


FIG. 11: Nature of expansion, shear and rotation for  $f(\sigma) = -\log(\cosh \sigma)$ ,  $a(\eta) = 2\eta$  and  $b(\eta) = 1 + 1/\eta$  with two different set of initial conditions. In (a) and (b), subscripts 0 ( $h$ ) correspond to zero (high) initial rotation.

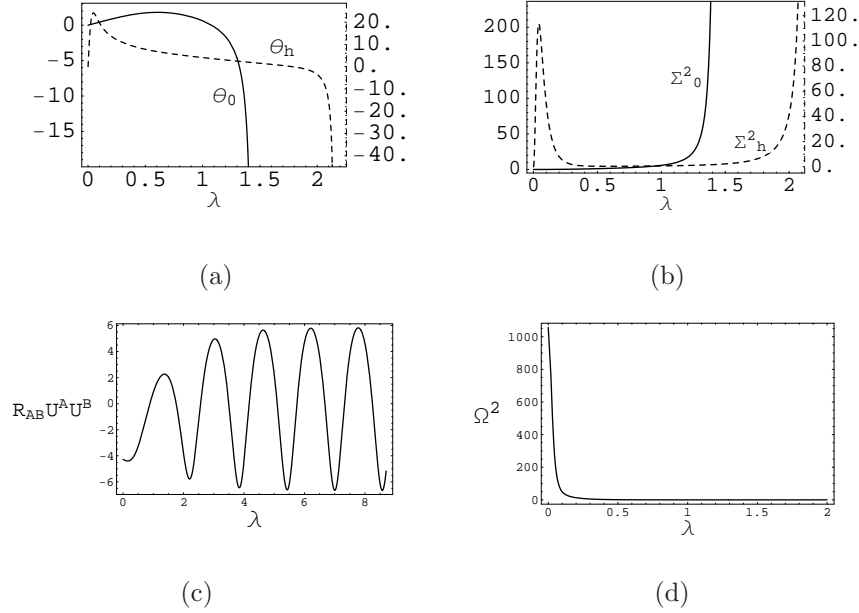


FIG. 12: Nature of expansion, shear and rotation for  $f(\sigma) = \log(\cosh \sigma)$ ,  $a(\eta) = 1/(1 - \eta)$  and  $b(\eta) = 1 - \eta/2$  with two different set of initial conditions. In (a) and (b), subscripts 0 ( $h$ ) correspond to zero (high) initial rotation.

rotation decays down very quickly. The physical reason behind this is the very fast expansion

of spacetime that smears out all the initial rotation components.

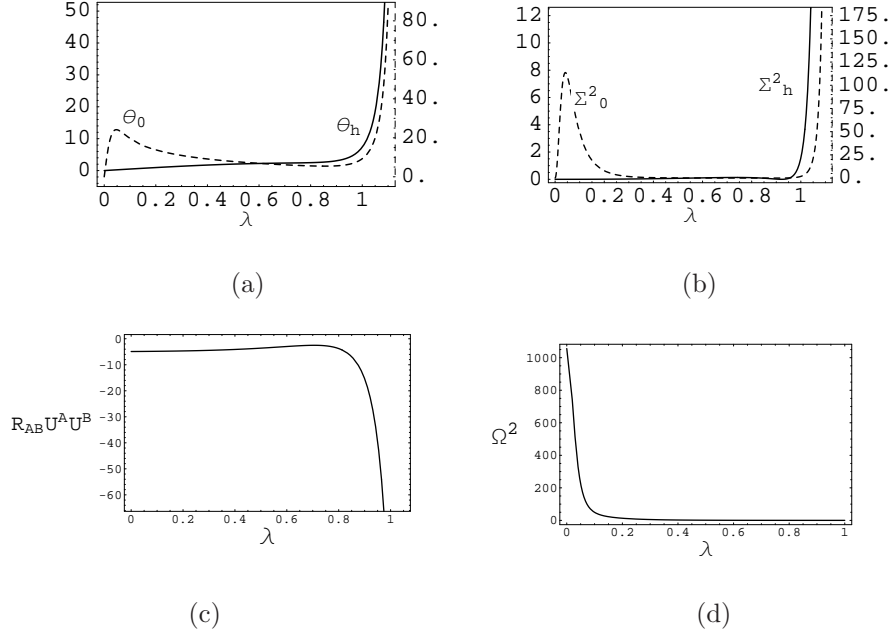


FIG. 13: Nature of expansion, shear and rotation for  $f(\sigma) = -\log(\cosh \sigma)$ ,  $a(\eta) = 1/(1 - \eta)$  and  $b(\eta) = 1 - \eta/2$  with two different set of initial conditions. In (a) and (b), subscripts 0 (h) correspond to zero (high) initial rotation.

Fig.13: In the presence of a decaying warp factor, a de Sitter brane with an asymptotically static extra dimension, we have an example where geodesics are defocused irrespective of initial rotation. Even though it seems that at late times shear totally dominates rotation, it is the curvature term in the Raychaudhuri equation that becomes dominant and causes the defocusing. Remember that, with  $a(\eta) = b(\eta) = \text{constant}$ , congruence singularity was inevitable (Fig.5). On the other hand, Fig.13(c) shows that initially the curvature term is very small, which implies that a high enough initial negative expansion should lead to a congruence singularity at a finite  $\lambda$  (before the curvature term becomes dominant). This behavior has been checked with an initial expansion,  $\Theta = -30$  (figure not shown).

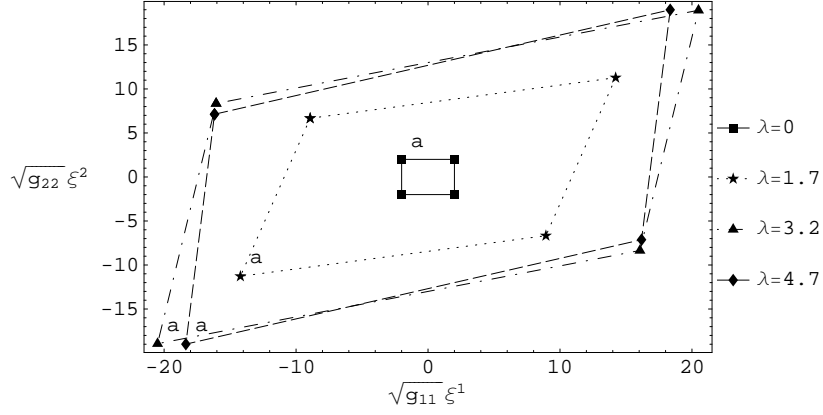
From the results in Fig.10-Fig.13, one can draw some general conclusions about the nature of the ESR variables. Congruence singularity is inevitable in the cases addressed in Fig.10 and Fig.12, i.e. for growing warp factor with Set(A) and Set(B) scale factors. Even a large amount of initial rotation fails to resolve the congruence singularity. This is because, in the presence of growing warp factor, the geodesics have a turning point in the extra dimension. This forces the congruence singularity to occur. Using different initial

conditions for the kinematic variables, such as high initial expansion will not resolve this congruence singularity. Fig.11 represents a case where the geodesics are not bounded. Even a high initial expansion cannot make the congruence to diverge. On the other hand, the geodesics are divergent when  $f(\sigma) = -\log(\cosh \sigma)$ ,  $a(\eta) = 1/(1 - \eta)$  and  $b(\eta) = 1 - \eta/2$  (Fig.13), which corresponds to a negatively warped and exponentially expanding brane. It is interesting to note that defocusing happens irrespective of the value of “ $\Omega^2$ ”. This is because the term, in the right hand side of Eq.3.6, “ $R_{AB}u^A u^B$ ” becomes dominant and large negative (which is not the case with other combinations of the metric functions) as  $\lambda$  increases (Fig.13(c)). Therefore, one can say that this defocusing is purely an effect of the spacetime geometry and the congruence singularity can arise with initially high negative expansion. Further, the dashed curves in Figs 10(a), 11(a), 12(a) and 13(a) show that even if we begin with a large initial rotation, in the end, shear dominates. Initially, expansion remains positive entirely due to high initial rotation.

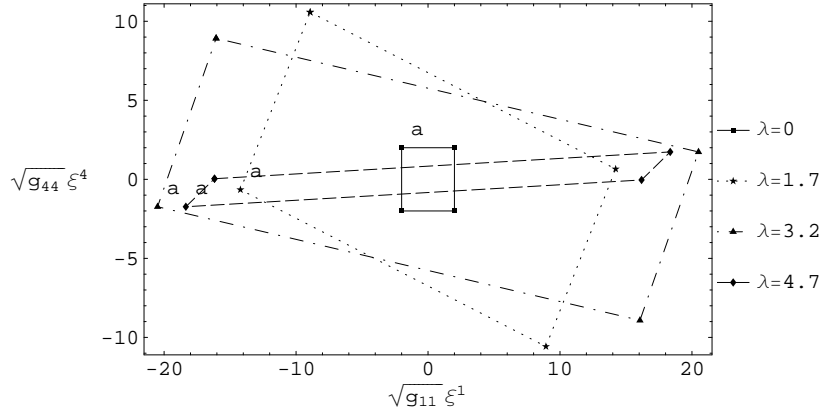
Let us now look at the evolution of a congruence of geodesics from the local observer’s point of view and see how the ESR profiles, plotted in Figs10-13, are realised. As done earlier, here also we have plotted the evolution of square elements, orthogonal to the congruence of the timelike geodesics, projected on  $\sqrt{g_{11}}\xi^1$ - $\sqrt{g_{22}}\xi^2$  and  $\sqrt{g_{11}}\xi^1$ - $\sqrt{g_{44}}\xi^4$  planes. These plots provide a different perspective of the evolution since they involve different shear and rotation tensor components. We have labeled one point of each area element (the one in the second quadrant, initially) as “a”. Following the location of this labeled point on future quadrilaterals (with increasing  $\lambda$ ) one can see the effect of rotation.

Fig.14 corresponds to the evolution of the dashed curve in Fig.10(a). Fig.14(a) suggests the following. Initially, the area element expands very quickly due to large amount of rotation—a feature clearly visible. At the end, rotation starts to increase again after slowing down a little in the middle and the area starts to shrink too. The amount of shear increases initially though towards the end it starts to decrease. In Fig.14(b) shrinking of the area element after an initial expansion, increase in the amount of shear after a decrease in the middle and a quick decrease in rotation are more clearly visible.

Fig.15 represents the evolution of the dashed curve in Fig.13(a). In both the plots, the area of the quadrilateral keeps on increasing with  $\lambda$ . Effect of high initial rotation is prominent, so is its rapid decrease. Effect of shear in Fig.15(b) matches with the profile of Fig.13(b), though this is not exactly the case with Fig.15(a). As mentioned earlier,



(a) Evolution of the projected square element on  $\sqrt{g_{11}}\xi^1$ - $\sqrt{g_{22}}\xi^2$  plane



(b) Evolution of the projected square element on  $\sqrt{g_{11}}\xi^1$ - $\sqrt{g_{44}}\xi^4$  plane

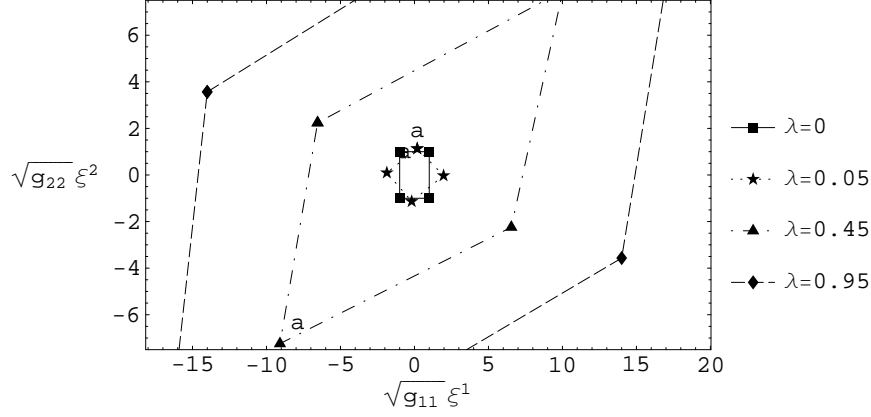
FIG. 14: Evolution of different 2D surface elements for  $f(\sigma) = \log(\cosh \sigma)$ ,  $a(\eta) = 2\eta$  and  $b(\eta) = 1 + 1/\eta$  with  $\Theta = \Sigma^2 = 0$  and  $\Omega^2 \sim 54$  at  $\lambda = 0$

these qualitatively different ESR evolutions are in one to one correspondence with different models. Therefore, loosely speaking, the pictorial visualisation provides pointers toward possible verification of those models, though much more needs to be done in order to arrive at explicit verifiable signatures.

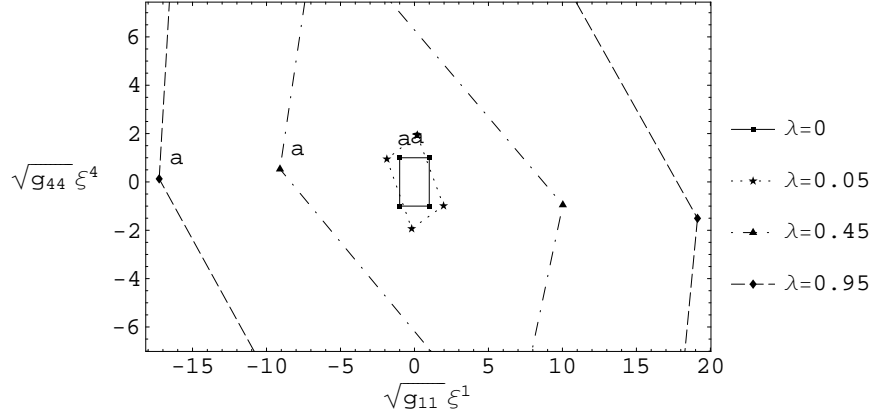
#### IV. DISCUSSION

In this article we have analysed, in detail, the kinematics of timelike geodesic congruences in a generalised bulk-brane scenario where we have a background five dimensional bulk





(a) Evolution of the projected square element on  $\sqrt{g_{11}}\xi^1 - \sqrt{g_{22}}\xi^2$  plane



(b) Evolution of the projected square element on  $\sqrt{g_{11}}\xi^1 - \sqrt{g_{44}}\xi^4$  plane

FIG. 15: Evolution of different 2D surface elements for  $f(\sigma) = -\log(\cosh \sigma)$ ,  $a(\eta) = 1/(1 - \eta)$  and  $b(\eta) = 1 - \eta/2$  with  $\Theta = \Sigma^2 = 0$  and  $\Omega^2 \sim 1080$  at  $\lambda = 0$

with a warped cosmological brane and an extra dimension whose size is time dependent. We now briefly summarize the work reported, the results obtained and possibility of future investigations.

- We initiate our discussion by looking at the simplest special case –the Randall Sundrum scenario (bulk Einstein space) with and without branes. In this case, the equations become analytically solvable when shear and rotation components are consistently assumed to vanish. Without branes things are simple and congruence singularities always arise. However, introduction of two branes (i.e. where the background is a slice of AdS spacetime) considerably changes the expansion profile of geodesic con-

Warp factor $e^{2f(\sigma)}$	Constant $a(\eta)$ , $b(\eta)$ (Analytical results)	$a(\eta) = 2\eta$ , $b(\eta) = 1 + 1/\eta$ (Radiative)	$a(\eta) = 1/(1 - \eta)$ , $b(\eta) = 1 - \eta/2$ (de Sitter)
Growing	Congruence singularity at finite $\sigma$ (Fig.4)	Congruence singularity at finite $\sigma$ (Fig.10)	Congruence singularity at finite $\sigma$ (Fig.12)
Decaying	Congruence singularity at $\sigma \rightarrow \infty$ (Fig.5)	Congruence singularity at $\sigma \rightarrow \infty$ (Fig.11)	Defocusing at $\sigma \rightarrow \infty$ (Fig.13) or congruence singularity at finite $\sigma$ for large, -ve initial $\Theta$
Constant	–	No congruence singularity (Fig.8)	No congruence singularity (Fig.9)

TABLE I: Summary of behaviour of geodesic congruences for different metric coefficients

gruences because of the presence of boundaries. Depending on the values of the new parameters introduced (i.e. the initial conditions) both focusing and defocusing can arise in the region between the branes. We also point out, through a parameter space diagram, which initial conditions in parameter space give rise to focusing/defocusing of congruences. This discussion (Section III A) therefore shows how extra dimensions and branes can have an effect on families of geodesics.

- In Section IIIB we work with thick branes in the generalised bulk-brane scenario. Different functional forms for the metric functions (namely  $f(\sigma)$ : the warp factor,  $a(\eta)$ : the cosmological scale factor and  $b(\eta)$ : the scale factor attached with the extra dimension) are chosen keeping in mind physically relevant models. The four types of combinations used give us four different viable braneworld scenarios with a cosmological (thick) brane. The kinematics of geodesic flows in these backgrounds are first obtained analytically, for restricted cases, using the first integrals of geodesic motion. The analytic expressions for the kinematic variables help us explicitly distinguish between the effects of varying the individual metric functions. Differences arise while we change the warp factor from growing to decaying or when we do not have any warping but retain the time-evolving cosmological and extra dimensional scales. What is important here is the fact that from the behaviour of families of trajectories we may be able to conclude about the nature of the metric functions, at least in qualitative

terms.

- Finally in Section IIIC we numerically solve the Raychaudhuri and the geodesic equations to arrive at the profiles of the expansion, shear and rotation. Once again, the interplay among different metric functions e.g. effect of warping and cosmological expansion of the brane is clearly visible in the results. In addition, we can now reflect on the role of initial conditions on the evolution of the kinematic variables. In general, we note that a growing warp factor leads to a finite  $\eta$  (and  $\sigma$ ) congruence singularity whereas in the presence of a decaying warp factor, geodesics are focused at  $\eta$  (and  $\sigma$ )  $\rightarrow \infty$ . In a radiative universe (where  $a(\eta) \sim \eta$ ), the above qualitative picture holds. However, in a de Sitter universe (where  $a(\eta) \sim 1/(1 - \eta)$ ), a decaying warp factor may fail to focus the geodesics (due to the large negativity of the curvature term in the Raychaudhuri equation), though this is not the case with a growing warp factor. When the curvature effect is relatively small, a congruence singularity can arise but for high enough negative initial expansion.

The effect of initial rotation, on the ESR profiles, especially the expansion scalar, is found to be quantitative. In cases with focusing without any initial rotation as well as with large initial rotation, similar results are obtained, though with large initial rotation, geodesics tend to spread for a while (focusing at larger  $\lambda$  value). The above conclusions are summarised in Table I.

- In order to provide a visual perspective, we have plotted the snap-shots in the evolution of a square element which represents the surface orthogonal to a geodesic congruence, from a local observer's point of view. The behaviour of the expansion, shear and rotation, along the congruences becomes more explicit through these graphs.
- The effect of a dynamic extra dimension i.e. the role of  $b(\eta)$  seems to be largely quantitative. This is because in these models as  $\lambda$  evolves  $b(\eta)$  tends to a static value with a deceleration. For a different dynamic nature of the extra dimension one is bound to get different results, a consequence we have not explored here.

In our work here, we have considered congruences of timelike geodesics and analysed their kinematical features (focusing/defocusing, shear and rotation evolution). It may be asked—what relevance, if any, does a congruence singularity have in the context of realistic

scenarios? After all, congruence singularities are not real spacetime singularities where curvatures diverge. Here, we are tempted to draw an analogy from null geodesic congruences, for which congruence singularities are nothing but the well-studied caustics where optical intensities get magnified immensely. Similarly, in the case of timelike geodesics, we may end up with accretion-like effects resulting out of matter accumulation in the neighborhood of a point. For instance, our visualisation analyses do show how the square elements change shape, get rotated because of variations in the metric functions. We may contemplate such accretion effects for flows around brane-world black holes [28] and in such situations, it will become necessary to pursue a line of thought very similar to what we have followed in this article. We hope to return to these issues at a later stage, in future.

### Acknowledgments

SG thanks Council for Scientific & Industrial Research (CSIR), India for providing financial support and Centre for Theoretical Studies, IIT Kharagpur, India for allowing him to use its research facilities.

- 
- [1] Th. Kaluza, Sitzunober. Preuss. Akad. Wiss. Berlin, 966 (1921); O. Klein, Z. Phys. 37 (1926) 895
  - [2] M. S. Green, J. H. Schwarz and E. Witten, *Superstring theory* (Cambridge University Press, UK, 1987); J. Polchinski, *String theory* (Cambridge University Press, UK, 1997).
  - [3] I. Antoniadis, *A Possible new dimension at a few TeV*, Phys. Lett. B **246** (1990) 377.
  - [4] N. Arkani-Hamed, S. Dimopoulos, G. Dvali, *The hierarchy problem and new dimensions at a millimeter*, Phys. Lett. B **429**, 263-272 (1998); N. Arkani-Hamed, S. Dimopoulos, G. Dvali, *phenomenology, astrophysics and cosmology of theories with sub-millimeter dimensions and TeV scale quantum gravity*, Phys. Rev. D **59**, 086004 (1999).
  - [5] I. Antoniadis, N. Arkani-Hamed, S. Dimopoulos and G. R. Dvali, *New dimensions at a millimeter to a Fermi and superstrings at a TeV*, Phys. Lett. B **436** (1998) 257 [arXiv:hep-ph/9804398].
  - [6] L. Randall and R. Sundrum, *A large mass hierarchy from a small extra dimension*, Phys. Rev.

- Lett. **83**, 3370 (1999).
- [7] L. Randall and R. Sundrum, *An alternative to compactification*, Phys. Rev. Lett. **83**, 4690 (1999).
  - [8] S. Ghosh, S. Kar and H. Nandan, *Confinement of test particles in warped spacetimes*, Phys. Rev. D **82**, 024040 (2010) [arXiv:0904.2321 [gr-qc]].
  - [9] S. S. Seahra, *Classical confinement of test particles in higher dimensional models: Stability criteria and a new energy condition*, Phys. Rev. **D68**, 104027 (2003).
  - [10] A. K. Raychaudhuri, *Relativistic cosmology. I*, Phys. Rev. **98**, 1123 (1955);
  - [11] S. W. Hawking and G. F. R. Ellis, *The large scale structure of spacetime* (Cambridge University Press, Cambridge, UK, 1973).
  - [12] R. Penrose, *Gravitational collapse and space-time singularities*, Phys. Rev. Lett. **14**, 57 (1965).
  - [13] S. W. Hawking, *Occurrence of singularities in open universes*, Phys. Rev. Lett. **15**, 689 (1965); *Singularities in the universe*, *ibid* **17**, 444 (1966).
  - [14] E. Poisson, *A relativists' toolkit: the mathematics of black hole mechanics* (Cambridge University Press, UK, 2004).
  - [15] R. M. Wald, *General Relativity* (University of Chicago Press, Chicago, USA, 1984).
  - [16] P. S. Joshi, *Global aspects in gravitation and cosmology* (Oxford University Press, Oxford, UK, 1997).
  - [17] G. F. R. Ellis in *General Relativity and Cosmology, International School of Physics, Enrico Fermi-Course XLVII* (Academic Press, New York, 1971).
  - [18] I. Ciufolini and J. A. Wheeler, *Gravitation and inertia* (Princeton University Press, Princeton, USA, 1995).
  - [19] S. Kar and S. SenGupta, *The Raychaudhuri equations: a brief review*, Pramana **69**, 49 (2007); gr-qc/0611123 and references therein; S. Kar, *Introducing the Raychaudhuri equations*, Resonance, Journal of Science Education **13**, 319 (2008).
  - [20] A. Dasgupta, H. Nandan and S. Kar, *Kinematics of geodesic flows in stringy black hole backgrounds*, Phys. Rev. D **79** 124004 (2009).
  - [21] A. Dasgupta, H. Nandan and S. Kar, *Kinematics of deformable media*, Annals of Physics **323**, 1621 (2008); arXiv: 0709.0582.
  - [22] A. Dasgupta, H. Nandan and S. Kar, *Kinematics of flows on curved, deformable media*, Int. J. of Geom. Meth. Mod. Phys. **6(4)** (2009); arXiv: 0804.4089.

- [23] R. Koley and S. Kar, *Scalar kinks and fermion localisation in warped spacetimes*, Class. Quant. Grav. **22**, 753 (2005) and references therein.
- [24] P. Kanti, K. A. Olive and M. Pospelov, *Static solutions for brane models with a bulk scalar field*, Phys. Lett. B **481**, 386 (2000).
- [25] V. Dzhunushaliev, V. Folomeev and M. Minamitsuji, *Thick brane solutions*, Rept. Prog. Phys. **73**, 066901 (2010) [arXiv:0904.1775 [gr-qc]].
- [26] S. Ghosh and S. Kar, *Bulk spacetimes for cosmological braneworlds with a time-dependent extra dimension*, Phys. Rev. D **80**, 064024, (2009).
- [27] T. C. Scott and R. B. Mann, *General Relativity and Quantum Mechanics: Towards a Generalization of the Lambert W Function*, AAEECC (Applicable Algebra in Engineering, Communication and Computing), vol. 16, no. 6, (2006) [arXiv:math-ph/0607011v2].
- [28] C. S. J. Pun, Z. Kovacs and T. Harko, *Thin accretion disks onto brane world black holes*, Phys. Rev. D **78** (2008) 084015 [arXiv:0809.1284 [gr-qc]].